Temporal dynamics of storage ring free electron lasers

M. E. Couprie,[1,2] T. Hara,[1,2] D. Gontier,[3] P. Troussel,[3] D. Garzella,[1] A. Delboulbé,[1] and M. Billardon[1,4]
[1]*Commissariat à l'Energie Atomique, DSM DRECAM SPAM, Cen-Saclay, 91191 Gif Sur Yvette, France*
[2]*Laboratoire pour l'Utilisation du Rayonnement Electromagnétique, Bâtiment 209 D, Université de Paris-Sud, 91405 Orsay Cedex, France*
[3]*Commissariat à l'Energie Atomique Centre de Limeil-Valenton Boîte Postale 27, Villeneuve-St. Georges 94193, France*
[4]*Ecole Supérieure de Physique et de Chimie de la Ville de Paris, 10 rue Vauquelin, 75231 Paris Cedex 05, France*
(Received 14 August 1995)

The growth and saturation of a storage ring free electron laser (SRFEL) is driven by the beam behavior, including bunch lengthening or coherent modes of longitudinal motion (the bunch length being related to the energy spread), detuning effects, and modification of the bunch distribution by the FEL interaction; all of these phenomena are accumulated for various passes, leading to complex dynamical processes. The knowledge and understanding of the dynamics, together with the stability over time are essential for efficient use of SRFEL sources. This is illustrated with the Super-ACO FEL experiment, analyzed from growth from the positron bunch to laser saturation and induced positron beam modification. Stability analysis (jitter, shape, intensity) is then performed carefully. A longitudinal feedback system can significantly improve it. Information provided with a streak camera reveals the distribution of a single FEL micropulse or synchrotron radiation pulse without any averaging or sampling.

PACS number(s): 41.60.Cr

I. INTRODUCTION

A. General motivation for the study of the temporal stability for a storage ring free electron laser (FEL) source for users

FELs are coherent, tunable, pulsed light sources, first demonstrated nearly 20 years ago [1]. Largely developed in the infrared where the gain is rather high, several user facilities based on linear accelerator or a Van de Graaff accelerator are spread over the world in such a spectral range. As far as the uv is concerned, the gain drops and high beam quality is required, leading to the use of storage rings [2–5] or recent and challenging technologies of photoinjector and microundulator on linear accelerators [6]. Table I compares the different performances of such sources, and mentions the projects underway. Storage ring FELs now provide reliable FEL sources for use, especially on (UVSOR) [4] and on Anneau de Collisions d'Orsay (Super-ACO) i.e., Orsay collision ring [2], where dynamics is actively studied. The operating conditions of Super-ACO for the FEL are now more or less compatible with the users of synchrotron radiation, taking advantage of its temporal structure in the two bunches mode, opening the possibility of designing a synchrotron radiation center that offers a variety of tunable [infrared (IR) to x rays] radiation from bending magnets and high brilliance insertion devices to a more powerful, tunable, and coherent FEL source, which can easily be coupled to synchrotron radiation [7]. The first experiments performed on the Super-ACO FEL [8,9] demonstrate that a stage of maturity has been reached, and that storage ring FELs in the uv-vuv range are competitive compared to conventional lasers. Nevertheless, the stability is a critical issue for operating a storage ring FEL as an user source: both longitudinally and transversally, for temporal scales ranging from the ps scale (the micropulse duration range) to half an hour (a typical user data acquisition time). These features will be discussed mainly on the Super-ACO FEL, but the different theoretical explanations related to the experimental results can reasonably be extended to the other projects or facilities.

B. Recall of the fundamental principles of FELs

The amplifying system results from the interaction of relativistic electrons in a permanent periodic magnetic field with the optical waves. The electron beam passes through the sinusoidal vertical magnetic field of the undulator, emitting synchrotron radiation on the fundamental wavelength λ and its harmonics according to

$$\lambda=\frac{\lambda_0}{2\gamma^2}(1+K^2/2)\,, \tag{1}$$

with λ_0 the spatial period of the undulator, the deflection parameter $K=0.94\ [\lambda_0\ (\mathrm{cm})]\ [B_0\ (\mathrm{T})]$, B_0 being the peak magnetic field of the undulator, and γ the normalized energy of the particles. By storing this radiation in an optical cavity, and by ensuring a proper synchronization between the positron bunches and the optical pulses (so-called "detuning"), the energy exchange occurring between them into the undulator can lead to light amplification, to the detriment of the kinetic energy of the electrons and to the laser effect. Such sources are simply tunable by a simple modification to the magnetic field of the undulator. The laser transverse-electromagnetic mode is generally TEM_{00}, defined by the design of the optical cavity. The 10-h duration of the uv Super-ACO FEL for an injected positron beam of 120-mA at 800 MeV, and the reasonable output power (100

TABLE I. List of uv storage ring free electron laser facilities.

FEL	Location	Date	Energy (MeV)	Spectral width (Å)	Spectral range (nm)	P (mW/ 10 mA)	Pulse duration FWHM separation	I (mA)	t (h)	Gain (%)	Remarks
VEPP3	CEI, Novosibisrk	1978–1994 laser 1988	350	0.01	690–580 460–375 270–240	3 1	90 ps/125 ns	20 20	0.5	10	Different optical klystron, linewidth narrowing, *shortest* λ.
Super-ACO	Orsay, France	1988–? laser 1989 uv 1991	600 600 700 800	0.4	690–606 345–355	24 10 180 540	50 ps 120 ns	2×45 2×30 2×22 2×60	2 5.5 12	2	Short micropulse, *first user experiment.*
UVSOR	Okazaki, Japan	1988–? laser 1992	500		488 300	1	15 ps/178 ns	10	1	0.4 0.7	Gain improvement with a 2nd rf cavity.
NIJI-4	Tsukuba, Japan	1990–? laser 1992 uv 1994	240		595 353	low	50 ns		1	5–10	First dedicated SR FEL, SR built by Kawasaki H. Ind.
DELTA	Dortmund, Germany	1989–?	500–1500		visible uv					> 10	Dedicated facility, 1994: commissioning.
Duke	N. Carolina, USA	1989 transfer from Stanford	1000		visible vuv					> 10	1994: commissioning dedicated facility,
KEK	Tsukuba, Japan	1991	750		177					10	1992: installation of the optical klystron.
FELI	Hirakata, Japan	1992	700		200						Common installation with IR LINAC FELs.
NIKHEF	Amsterdam, NL	1993	900		vuv						Nondedicated,
EUTERPE	Eindhoven, NL	1993	400		xuv						Nondedicated facility.
SOLEIL	France	1993	1500 2150 ring		350–100	1 W		4×10 m *A*	> 5	> 10	Synchrotron radiation facility FEL on 14-m-long straight sections at 1.5 GeV.
Diamond	Daresbury, GB	1993	700		xuv						Not yet funded.

mW of available output power, the highest for uv FELs) made the dynamical studies, including streak camera experiments, rather easy to perform.

C. First applications of storage ring FELs

Dynamical studies are really motivated by the improvement of the SRFEL sources for users, and the first applications carried out on Super-ACO pointed out some critical stability requirements. So far, the feasibility of using the Super-ACO storage ring as a uv light source was demonstrated with the study of polarized fluorescence decays of the reduced nicotinamide adenine dinucleotide coenzyme in aqueous solution, using the single photon counting (SPC) technique [8]. A complete fluorescence experiment required about 30 min of data acquisition, during which the best integrated instrumental response had a full width at half maximum (FWHM) of 110 ps with fluctuations of the absolute position of the apparatus function smaller than 5–10 ps, and a high number of counts (10^5 at the maximum). The temperature dependence of the two measured lifetime components led to the thermodynamical parameters of the conformational equilibrium, in good agreement with other spectroscopic techniques. The fluorescence anisotropy decays versus temperature provides an apparent hydrodynamic radius of the folded form (in good agreement with the results obtained with the method of van der Waals) and indicates a fast independent motion of the nicotinamide ring. The quality of the collected data fully meets the requirements for the study of more complex systems, such as fluorescent compounds bound to proteins or membranes.

Moreover, pump-probe experiments are now underway, using both the uv FEL and the synchrotron radiation from the Super-ACO storage ring, both naturally synchronized, polarized, and tunable: the dynamics of the intermediate state excited by the pump beam and characterized by the probe source being analyzed by varying the delay between the two-light source (between 1 and 120 ns Super-ACO). Such a pump-probe technique opens a wide field of applications for storage ring FELs, where synchrotron radiation covers from the infrared to x rays, and can be applied to various scientific fields. The first results were obtained in interface physics for the study of the surface photovoltage effect at the semiconductor-metal interface [9–11]. Other experiments are planned for the photoionization of excited helium [9] or FEL induced excitation of photocarriers and creation of photofragments probed by infrared synchrotron radiation [9]. Such experiments provide a challenging issue for storage ring FEL sources in the uv, with the specificity of combining synchrotron radiation.

It is then essential to follow the evolution of the temporal features of such sources, and to understand how the dynamics takes place for this complex system. This paper deals with the specificities of FEL dynamics on a storage ring, with a particular interest on the evolution of the temporal parameters of the source, starting from the bunch at the origin of the FEL interaction to the FEL micropulse, and its stabilization. It is illustrated on the super-ACO FEL case, with, of course, a description of the employed experimental system of temporal characterization.

II. GENERAL FEL TEMPORAL CHARACTERISTICS

SRFEL has a pulsed structure at a high repetition rate, resulting from the passes of the stored bunches in the storage ring, but it can produce series of macropulses at the ms range, depending on the detuning (synchronization between the electron bunches circulating in the ring and the optical pulses bouncing in the optical cavity) and the stability of the various components involved in the laser oscillation (electron beam, thermal distortion of mechanical equipment, etc.). Table II gathers the microtemporal characteristics of the uv SRFELs.

A. FEL microtemporal structure

The temporal structure of a storage ring FEL first results from that of the electron beam from which it is generated; generally, with a small number of stored bunches in order to avoid the bunch to bunch longitudinal oscillations, leading to a rather high repetition rate (of the order of the MHz). The FEL micropulse duration is 5 to 20 times shorter than the electron bunch, because the amplification occurs for the maximum of electronic density (see Table II). On Super-ACO, the two bunches of 90 to 300 ps rms, depending on the current, lead to a FEL micropulse of 50 ps FWHM in average for perfect tuning [12], with the presence of a jitter reaching values as big as 200 ps. It can be noticed that, on UVSOR, the use of a harmonic cavity leads to 70 ps rms electron bunches and the FEL offers the shortest pulses (i.e., 15 ps FWHM). Nevertheless, it would be difficult to reach the fms range, because of the associated reduction of Touschek lifetime associated with very short electron bunches; FEL driven by LINAC with a photoinjector should be preferable for that purpose.

B. FEL macrotemporal structure

Storage ring FELs can present, in addition to the ps structure, a macrotemporal behavior at the ms scale, either for bad beam stability of for particular conditions of detuning, with a natural frequency depending on the laser risetime and the synchrotron damping time (see Table II) or synchronized on line, on its multiples and harmonics. It results from a kind of oscillations of relaxation between the laser rising intensity and the energy enhancement damped in the ring [13]. This pulsed structure can also result from any type of instability, and is widely observed on storage ring FELs [2–5]. When the frequencies are close to a line or its harmonics, any line perturbation can drive the laser to a pulsed regime. With an artificial gain modulation, the laser can adopt a chaotic regime [14]; a high stability is thus imperatively required. The measurements with the streak camera are then possible because of the presence of these "continuous" regions of operation of the Super-ACO FEL (at perfect synchronism, and far from perfect synchronism); the high stability

could result from the use of positrons. On the UVSOR storage ring FEL [4], the laser is pulsed for perfect synchronism.

C. FEL behavior versus detuning

The dynamics of storage ring FELs is highly dependent on the tuning condition (synchronism between the optical pulses in the optical cavity and the bunches stored in the ring). When the stored beam is not very stable, coherent motion or rapid perturbations lead to a pulsed FEL at the ms range, as was usually observed in the first experiments. Nevertheless, the improvement of the beam stability with the newly built storage rings led to a reproducible behavior of the FEL macrotemporal structure versus detuning. On Super-ACO, one can distinguish five zones of operation (see Fig. 1) [15]. Around area 3 around perfect tuning, the laser power is maximum, the temporal and spectral widths of the laser micropulse are minimum, the temporal structure of the laser at the millisecond scale is cw, but the laser micropulse presents some jitter and intensity fluctuations. In the two adjacent zones (2 and 4), with a slight detuning, the laser is pulsed at the ms range, the widths of the distributions are enhanced, and the power is smaller. The presence of these two pulsed regions can be explained numerically in the Super-ACO FEL case [15]. For a larger detuning (areas 1 and 5), the laser is again cw at the ms scale, its power is reduced and the widths of the distributions are enhanced, but the laser micropulse is more stable in position and intensity; the FEL was operated under these conditions for time-resolved fluorescence experiment, because of the high stability requirements. On UVSOR, the cw central region is so tiny that only a main pulsed central region appears (corresponding to zones 2 and 4) surrounded by two detuned cw regions.

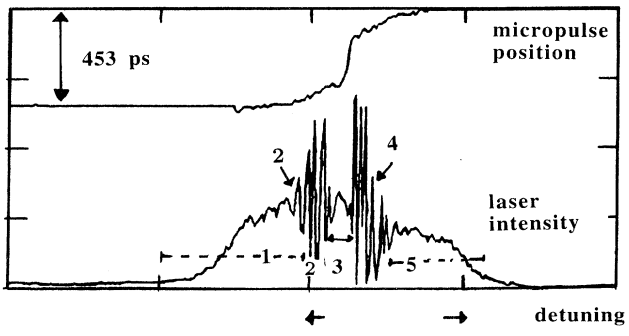

FIG. 1. Laser micropulse position (upper signal) measured with the dissector, as explained further, and intensity (lower signal) recorded with a photomultiplier versus detuning. One distinguishes five zones: three with a cw structure and two pulsed regions from both sides of perfect synchronization. The laser tuning is scanned by a linear ramp applied to the rf frequency modifying the synchronization between the electron bunch and the optical pulses (180-μm changes on the optical cavity length corresponds to 1 kHz).

TABLE II. Temporal structure of existing storage ring FELs.

Experiment	rms bunch length (ps)	rms laser pulse duration (ps)	Repetition rate (ns)	Laser rise time (μs)	Synchrotron damping time (ms)	Natural laser frequency (Hz)
Super-ACO	90–300	20	120	80	8	350
UVSOR	57–130	6	178	200	30	125
VEPP3	900	90	125			
NIJI-4			50		47	500

III. EXPERIMENTAL SETUP AND DATA TREATMENT

Besides a fast photodiode, two types of picosecond diagnostics can be used: dissector sampling the distribution and streak cameras in order to characterize the FEL micropulse and the electron bunch. The energy spread of the beam can be optically measured with the spectrum of the optical klystron, as described here.

A. Dissector

The dissector is a stroboscopic picosecond detector [16,17] developed at Novosibirsk for the measurement of periodic events, such as FEL micropulses or synchrotron radiation. The device is sketched in Fig. 2. The incident light is focused onto the photocathode, which transforms it into a temporal distribution. The electron beam is then deflected onto a slit plane by a high frequency voltage synchronized with the recurrence of the pulses. A certain part of the electron bunch distribution passes through the slit, whose width mainly determines the temporal resolution of the device (of the order of 10–15 ps). The electron passing through the slit are amplified with a system of dynodes, and transformed into an electric signal, which is sent to an oscilloscope. By adding a low frequency scanning voltage to the deflection plates, the whole distribution can be scanned through the slit. The sampling is generally performed at 50 Hz, but was recently increased to 1 kHz for faster detection. The optical alignment system with a lens and an iris before the photocathode has been changed recently into a cylindrical lens with a slit, in order to keep the same resolution, whatever the position of the incident light might be. The dissector calibration has been checked with an optical delay. The advantage of the dissector is to provide an electrical signal that well suitable for feedback systems; but a unique pulse distribution cannot be observed.

B. Streak camera

1. *Experimental setup*

The streak camera (Thomson TSN 506 with a uv S20 tube) from Commissariat à l'Energie Atomique-DAM (Centre of Limeil-Brévannes) was installed in Orsay on the Super-ACO FEL for two series of experiments of a few months each [13]. Several calibrations can be used: 10, 5, 2, and 1 ns (35 ps/mm), for a phosphorent screen of 4 cm. The laser micropulse extracted from the rear mirror of the optical cavity or the focused synchrotron radiation from a bending magnet can be alternatively sent on the dissector or the streak camera (see Fig. 3). The FEL light is selected from the stored spontaneous emission with an UG11 filter. The light is focused on the entrance slit of the streak camera with a cylindrical lens, and onto the photocathode with a uv entrance objective. Both optical beams can also be switched to the dissector.

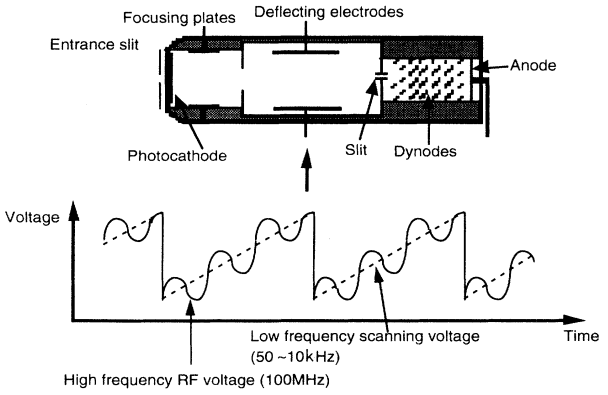

FIG. 2. Principle of the dissector.

2. *Synchronization*

The camera has been synchronized with a clock at 4.17 MHz (corresponding to the revolution frequency) delivered by the 100-MHz rf cavity of the storage ring [12], the signal being noncurrent dependent as in the pick-up electrode signal case. A lock-in system synchronizes the high repetition rate pulses with the trigger of the camera at 1 Hz. This limited recurrence, at a maximum of 10 Hz, has been chosen in order to protect the sweeping circuit. However, pulses are arriving on the tube at 8.17 MHz, and it limits the sensitivity of the camera (see Fig. 4). The installation of a rapid shutter could solve this problem. The operation of the FEL in the Q-switched mode requires an additional synchronization for the laser macropulses. With a double sweep streak camera, micropulse or even spectral features [4] can be measured versus the FEL macropulse, as performed on UVSOR.

3. *Data analysis*

The images are collected on 2484 films, then revealed, analyzed with a microdensitometer [12,18], and the data are treated using the specific computer code developed for this purpose on a VAX station computer, in ADONIS, a language developed in Limeil [18]. The distributions are analyzed using the moments M_i methods, providing the center of mass of the distribution with M_1, the root mean square with M_2, the dissymmetry with $M3$ without a Gaussian assumption (see Fig. 5). The smaller calibration is used for the analysis of one laser micropulse, in or-

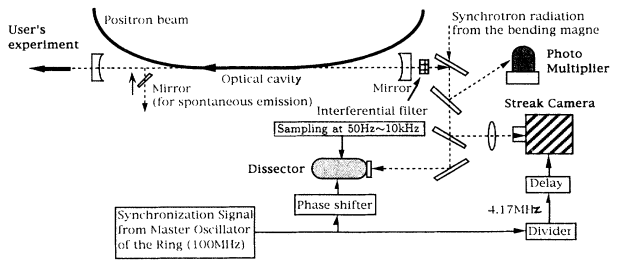

FIG. 3. Layout of the experiment.

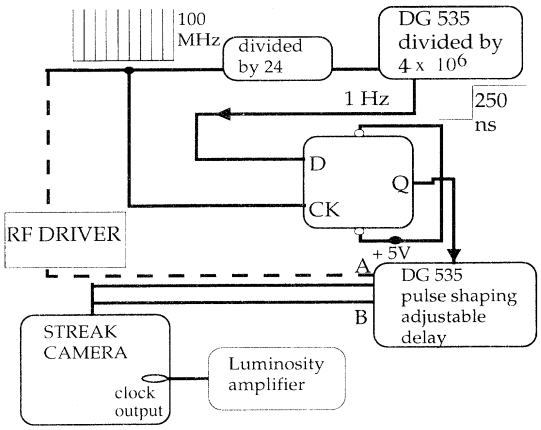

FIG. 4. Principle of the synchronization. A Stanford DG 535 pulse-shaping adjustable delay gives the 1-Hz synchronization signal from the 4.17 MHz by division per 4×10^6. This signal is compared to a clock pulse with rocking-lever *D*, delivering a very stable signal. A second Stanford DG 535 generator reshapes the signal and provides a very stable synchronization signal (jitter smaller than 50 ps). It also allows the synchronization signal to be artificially delayed between 100 ps and a few ms, in order to record several micropulses (FEL or synchrotron radiation) on the same film. For measuring the FEL in the *Q*-switched mode, the synchronization is indicated with dashed lines: the stable output *A* is sent on the rf pilot with optical fibers PCS 600 (Toshiba transmitter-receiver) to ensure the good transmission of the signal on long distances, in order to kill the laser gain for a few ms. A second output *B* triggers the camera after being artificially delayed by roughly 50 ms, corresponding to the laser rise time, delay after the reestablishment of the gain.

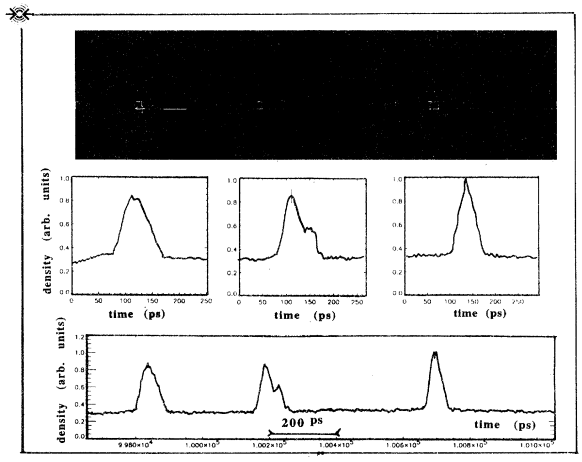

FIG. 5. Example of density profile and intensity laser distribution, this latter analyzed by the moments method. Several FEL micropulses are viewed, which were registered after applying an artificial delay.

der to exploit the 10-ps resolution of the detector. Several pulses, artificially delayed, can be recorded with a larger calibration.

C. Energy spread measurement

The energy spread is an important beam parameter to follow because it is directly modified by the FEL interaction and it is strongly related to the electron longitudinal distribution. It can be measured with the horizontal beam size in a location with a dispersive function. Another very precise method is provided by the spectrum of the optical klystron, specifically designed to enhance the FEL gain compared to the simple undulator configuration [19] for a rather short available straight section of the ring. It is constituted of two identical undulators of N periods separated by a dispersive section, creating a large wiggle of magnetic field, introducing the interference order N_d between the two undulators. The obtained radiation results from the interference from the undulators, as for two Young slits in optics. An example of the spectrum is given in Fig. 6(a). The equivalent of the optical contrast is the modulation rate f, mainly determined by the energy spread of the beam (σ_γ/γ),

$$f=f_0\exp[-8\pi2(N+N_d)^2(\sigma\gamma/\gamma)^2]\ , \tag{2}$$

f_0 being the residual modulation rate due to other contributions. Since the gain is the derivative of the spontaneous emission [20], it is enhanced with this fringe structure.

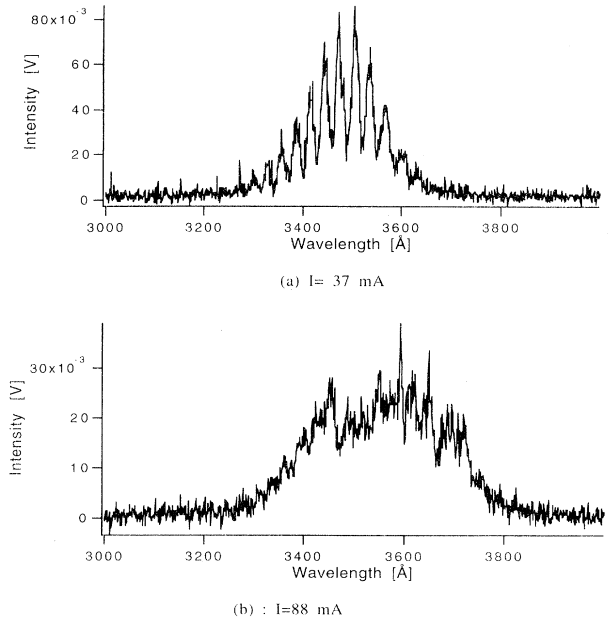

FIG. 6. Spontaneous emission of the optical klystron. The radiation from the two undulator interferes, as from two Young slits. (a) $I=37$ mA case of a stable beam, with a modulation rate of 0.58, $N+N_d=114$, resonant wavelength of 350 nm. (b) $I=80$ mA in the presence of quadrupolar modes: the spectrum is clearly distorted.

IV. TEMPORAL FEATURES OF THE SUPER-ACO FEL MICROPULSE

A. Origin: the longitudinal distribution of the positron bunch without laser

The longitudinal bunch distribution determines, to some extent, the laser longitudinal parameters, the gain of the system, etc. Its modification in presence of the FEL interaction results from the laser saturation. The laser does not grow from noise but from synchrotron radiation in the undulator, presenting some preliminary coherence: spatially (due to the low emittance beam in Super-ACO, i.e., $\mathcal{E}_x = 40$ nmrad) and longitudinally ($\Delta\lambda/\lambda = 1/N$, i.e., 5×10^{-2} for 20 periods in the Super-ACO case). Roughly, the laser is achieved after one thousand passes in the optical cavity.

1. *Bunch length at zero current*

The longitudinal motion of an electron in a storage ring is described by the two following equations [21]:

$$\frac{d\tau}{dt} = -\alpha\varepsilon \ , \qquad \frac{d\varepsilon}{dt} = [eV(t) - U_{\text{rad}}]/E_0 T_0 \ , \tag{3}$$

with τ the temporal coordinate relative to the synchronous electron ($d\varepsilon/dt = 0$), $\varepsilon = \Delta E/E$ the relative variation of the energy, t the time, α the momentum compression factor, T_0 the revolution frequency, U_{rad} the radiated energy per turn, $V(t)$ the applied rf voltage, e the electron charge. It leads to a second order differential equation, with the "synchrotron" pulsation of oscillation Ω_S,

$$\Omega_S = (\alpha\varepsilon V'/E_0 T_0)^{1/2} \tag{4}$$

and the synchrotron damping time τ_S. Without any additional term, due to the stochastic emission of radiation, the Fokker-Planck equation leads to Gaussian longitudinal distributions. The rms bunch length s_1 is given by

$$\sigma_1 = (\alpha c/\Omega_S)\sigma\gamma/\gamma \ . \tag{5}$$

σ_1 is proportional to $(\alpha h/V)^{1/2}$ with $\sigma\gamma/\gamma$ the energy spread, h being the harmonic number of the rf frequency. Such a bunch length is measured at quasizero current, and is of the order of 90 ps rms on Super-ACO for nominal operation (800 MeV, $\alpha = 2.48\times10^{-2}$, $V = 170$ kV, $h = 24$).

Isochronous operation of the ring (the momentum compression factor being very small) is very attractive for providing short electron bunches, and then promising for FEL [22]. Bunches shorter than 50 ps could be obtained on Super-ACO but, unfortunately, with a rather poor beam lifetime or higher emittance. The natural bunch length could also be reduced by enhancing the harmonic number of the rf frequency and increasing its voltage, that is why a 500-MHz rf cavity was initially planned on Super-ACO, allowing it to provide 40-ps rms bunches. A harmonic cavity was installed on UVSOR [4], allowing it to shorten the bunches down to 50 ps.

2. *Effect of the beam current: apparition of coherent modes of synchrotron oscillation*

In fact, for a real beam of intensity I, the electromagnetic field induced by the beam itself, coupled with the impedance of the environment (rf cavity, discontinuity of vacuum chamber, resistive wall, broadband resonator, etc.) provides an external force to the previous equation of motion [23]. The stationary solution gives the so-called "potential well" distortion at rather low current (with a small modification of the bunch length). When the current gets higher, i.e., above the threshold of "anomalous bunch lengthening" (of the order of 8 mA/bunch on Super-ACO) [24], in the so-called "microwave instability regime," the electrons in the bunch start to move in response to the electromagnetic field perturbation [25]. In addition, they can also oscillate coherently close to their natural oscillation synchrotron frequency, and its harmonics. The modes of oscillations (dipolar, quadrupolar, hexapolar) depend on the beam current. The upper limit of current, when the beam becomes completely instable (100 mA/bunch on Super-

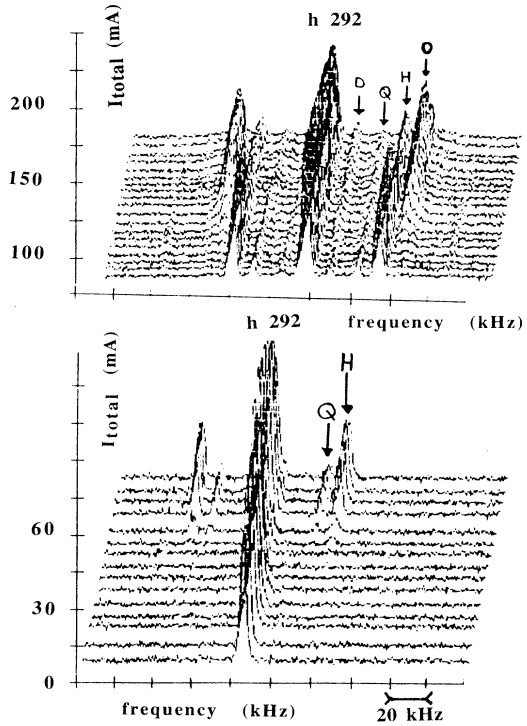

FIG. 7. Synchrotron modes of oscillations observed on the sidebands of a high harmonic of the revolution frequency (292), versus the stored current in two bunches on Super-ACO. There are octupolar modes (O) at 46.4 kHz, hexapolar modes (H) at 36 kHz, quadrupolar modes (Q) at 25.5 kHz, and dipolar modes (D) at 12 kHz (mainly damped with a feedback system). $E = 800$ MeV and Vrf = 170 kV.

ACO) provides the maximum current filling in the ring.

The coherent modes of oscillations can be visualized in the frequency space on a spectrum analyzer (Marconi) with synchrotron radiation collected by a pick-up electrode. The spectrum analyzer is centered on a high harmonic of the revolution frequency ($h=292$) and presents sidebands on the harmonics of the synchrotron frequency (of the order of 12 kHz). One can distinguish on Super-ACO several regimes versus current (see Fig. 7): 200 mA $< I <$ 130 mA, octupolar modes; 170 mA $< I <$ 80 mA, hexapolar modes; 110 mA $< I <$ 60 mA, quadrupolar modes; $I <$ 60 mA, stable beam (dipolar modes damped with a longitudinal feedback [26]). The current range is determined by the beam response to the oscillator, and depends on how it has been excited. For instance, a 70-mA beam can be stored on Super-ACO without quadrupolar modes of oscillations; they have not been excited yet. For some current range, several modes of synchrotron oscillations are simultaneously present. These modes can be represented in the phase and time spaces according to Fig. 8. The bunch is actually submitted to coherent modes of synchrotron oscillations [26], so to the following behavior in the bunch referential [21],

$$s = s_0 \sin(n\Omega_S t) \ . \tag{6}$$

The dipolar mode corresponds, for instance, to a rigid motion of the distribution, the quadrupolar to a long and flat form changing into a short and high form; hexapolar modes lead to clearly asymmetric shapes. The frequency of the quadrupolar mode is twice that of the dipolar modes because the elliptic shape in the phase scape has a twofold symmetry.

In the time domain, these coherent modes of oscillations can be observed with the dissector operating without ramping voltage (see Fig. 9) [27].

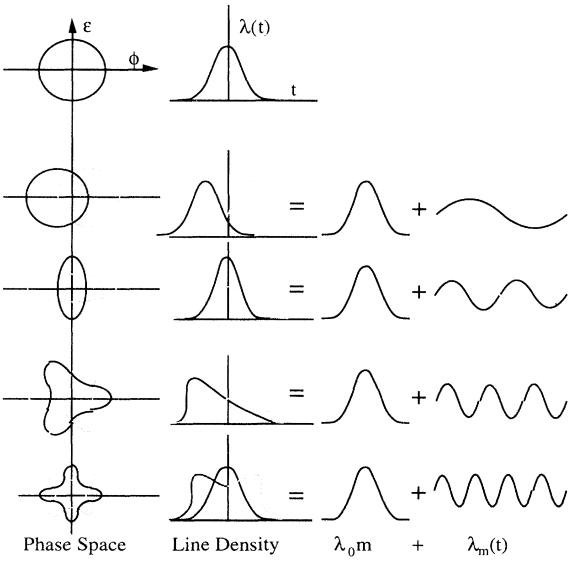

FIG. 8. Representation of the coherent synchrotron modes of oscillation in phase space and in time space.

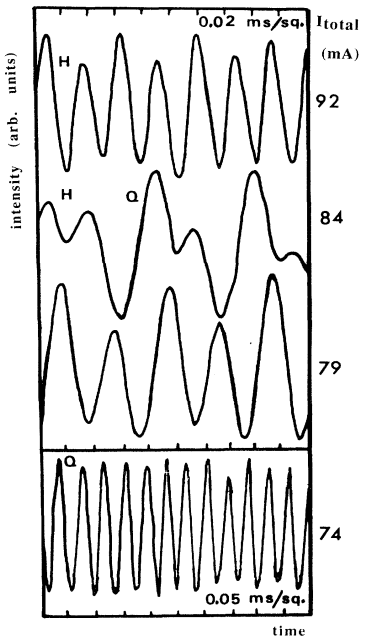

FIG. 9. Observation of the coherent modes of oscillations in the time domain with the dissector: in that case, the linear sweeping ramp voltage is not applied to scan the entire distribution, and the displacement of the distribution around the slit is recorded vs time. These coherent synchrotron oscillations could also be observed by recording the temporal evolution of the intensity of a fringe of the optical klystron.

3. *Evolution of the bunch distribution versus current*

The streak camera allows one to measure the shape of the longitudinal bunch distributions of single bunches versus current in the range where coherent synchrotron modes are present (see Fig. 10). Obviously, the bunch distribution is not Gaussian. Several records were performed for the same current and show some shape change, according to Fig. 8. One can distinguish the quadrupolar modes with a long (flat) shape evolving to a short (high) shape [see Figs. 1(h), 2(f), 2(h)] and sextupolar modes with clearly asymmetric shapes [see Figs. 1(d), 1(e), 2(b), 2(e), 2(f)], and octupolar modes with hollows sometimes [see Fig. 1(e)] and complex distributions. Various modes can be superimposed, so it might be more difficult to recognize the shape of the distribution. Such shape modification has been also observed at Berliner Elektronenspeicherring-Gesellschaft für Synchrotronstrahlung (BESSY) [28].

Figure 11(a) illustrates the rms values of the positron bunch distribution measured with the streak camera, and analyzed with the moments method. The dispersion of the data measured with the streak camera results from the rapid variation of the longitudinal distribution of the positron bunch. The values measured with the dissector are in rather good agreement. Dissector measurements here were not averaged on the oscilloscope, but over the

various records saved in the computer, and great care is taken on the data analysis. If not so, a greater discrepancy is found between the data, the wider values from the dissector measurements resulting from the averaging of the stroboscopic detection under the regime of turbulent motion of the particles in the bunch. The analysis of the moment of third order provides information about the asymmetry of the distribution measured with the streak camera, as shown in Fig. 11(b). The evolution of the bunch length versus I can be scaled for microwave instability as

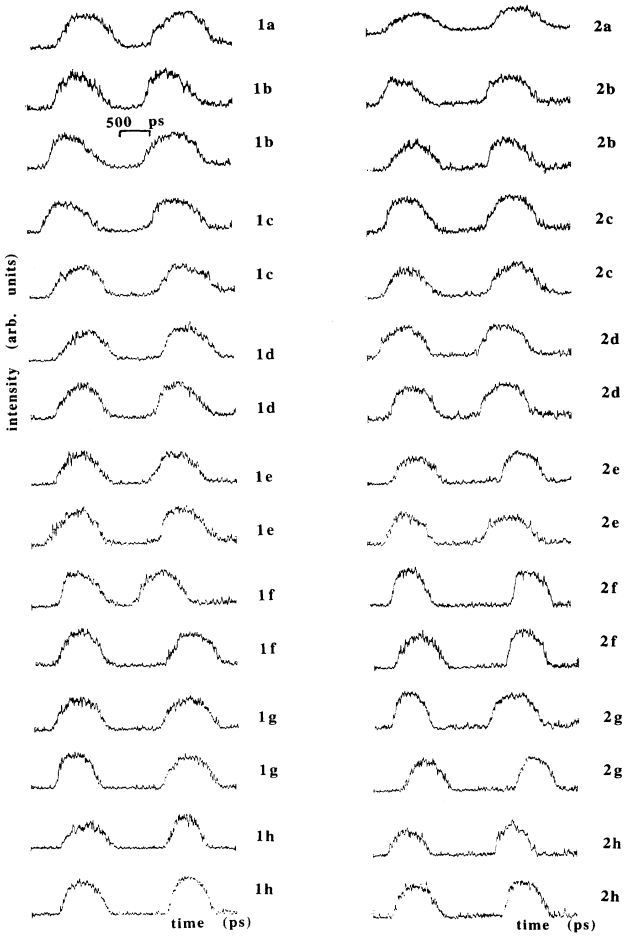

FIG. 10. Shape of the longitudinal bunch distribution vs current (streak camera measurements), for two series of measurements performed with the streak camera. 1(a) 172.4 mA (O), 1(b) 163.9 mA ($O+H$), 1(c) 149 mA ($O+H$), 1(d) 141 mA ($O+H$), 1(e) 129.3 mA ($O+H$) with a clear hole in the middle of the distribution, signature of an octupolar mode of oscillation, 1(f) 117.4 mA (H), 1(g) 109.8 mA ($H+Q$), 1(h) 98.8 mA (Q). 2(a) 156.8 mA (O), 2(b) 137.3 mA ($O+H$), 2(c) 126.3 mA ($O+H$), 2(d) 115.6 mA ($H+Q$), 2(e) 105.8 mA ($H+Q$), 2(f) 96 mA ($H+Q$), 2(g) 87.3 mA ($H+Q$), 2(h) 73 mA (Q). These experimental shapes should be compared to the theoretical ones in Fig. 8, according to the type of modes versus the current given in Fig. 7. (O for octupolar, H for hexapolar, Q for quadrupolar.)

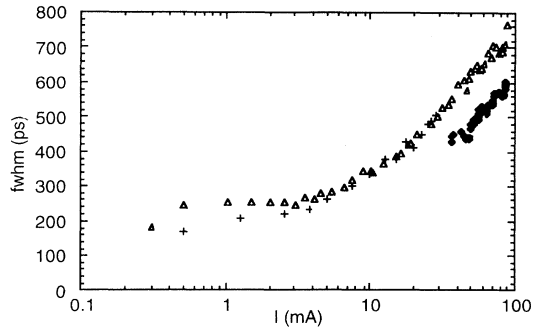

(a)

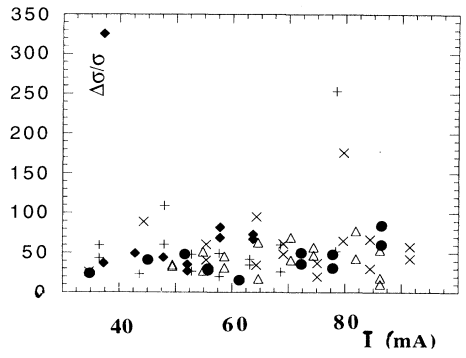

(b)

FIG. 11. Evolution of the positron bunch longitudinal distribution vs current per bunch in Super-ACO. (a) Streak camera measurements (squares) and dissector (at 800 MeV, triangles and at 600 MeV, crosses). (b) Streak camera measurements at 800 MeV: dissymmetry.

$$\sigma_1 a(\xi Z_0 R^3)^{1/(2+a)}, \tag{7}$$

with R the machine radius, Z_0 the impedance parameter, $\xi = I\alpha/\nu_s^2 E$, with α the momentum compression factor. The fit with the dissector gives $a = 0.79$ and 0.57 with the streak camera, not so far from $a = 1$, the limit for very long bunches [25,28]. The bunch length values are identical at 600 MeV down to $I = 3$ mA/b and at 700 MeV down to $I = 8$ mA/b, providing some information about the threshold of anomalous bunch lengthening, from which one could deduce the effective impedance.

4. Evolution of the energy spread versus current

The knowledge of the energy spread versus current is also a good diagnostic of the longitudinal behavior of the bunches. Figure 12 shows the evolution of the energy spread versus current measured with the spectrum of the optical klystron, and can be compared to Fig. 8. A strange behavior is observed below the threshold of microwave instability, with even a reduction of the energy spread when the current increases. With the spectrum of the optical klystron, the energy spread can be properly measured in the range of current where the dipolar

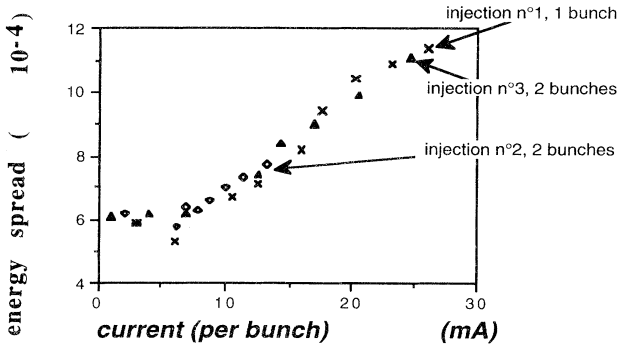

FIG. 12. Evolution of the energy spread of the bunch vs current, recorded with the fringes of the optical klystron spectrum.

modes of synchrotron oscillations are damped by the longitudinal feedback, but in presence of quadrupolar modes of coherent synchrotron oscillations, the optical klystron spectrum is completely modified [see Fig. 6(b)], because the distribution is moving and changing in shape during the acquisition time of the spectrum. The behavior of the energy spread and the bunch length are similar.

5. *Comparison of the operation with 24 bunches or 1 bunch*

For the 24 bunches operation of the Super-ACO, the coherent modes of synchrotron oscillations from the different bunches couple together, leading to a really unstable beam, due to the bunch to bunch longitudinal oscillations, and consequently, to jitters bigger than 1 ns (see Fig. 13). Besides, the operation in one single bunch of Super-ACO is analogous to that of the two opposite bunches stored in the ring, with the longitudinal feedback, the bunch to bunch interaction in that case being neglectable.

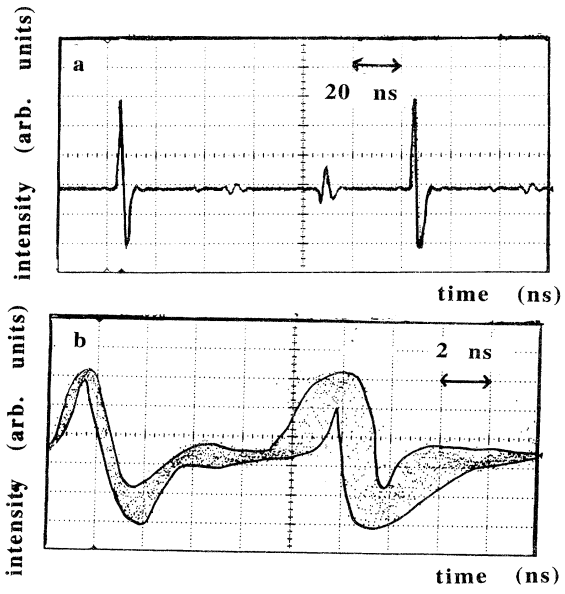

FIG. 13. Comparison of the stability with two stored bunches and 24 bunches observed with the signal from a pick-up station.

6. *Consequence for the FEL operation*

The synchronization condition between the positrons and the light pulses require a very stable beam, so two opposite bunches, stabilized by a longitudinal feedback [26], are stored for FEL operation. The presence of coherent synchrotron oscillations on the beam modifies completely the longitudinal bunch distribution (non-Gaussian, distorted spontaneous emission spectrum) and thus the gain, preventing the laser to start [29] or allowing it to work (with a rather high gain over cavity losses ratio), but in a rather unstable regime. As a consequence, the Super-ACO FEL is generally operated with two stored bunches below 70 mA, the threshold for quadrupolar and hexapolar modes of oscillations. A recent operation at 100 mA results from the improvement of the cavity losses, when the gain G over cavity losses P is not too small, leading to a laser risetime

$$\tau_r \sim T_0/2(G-P) \tag{8}$$

the laser can start, even in the presence of coherent synchrotron oscillations. It results also from the fact that the laser rising time (between 17 and 120 ms) and the synchrotron oscillation period are of the same order of magnitude. Probably, working with shorter synchrotron frequency would improve the situation. The synchrotron frequency can be reduced with the same means as the theoretical bunch length (isochronous operation, harmonic operation of the rf cavity).

B. FEL gain and saturation

1. *Gain*

The FEL gain in the optical klystron case is given by

$$G_0 = 1.12\times 10^{-13}(N+N_d)K^2 L_{0k^2} JJ^2 f F_f \rho/\gamma^3$$

with

$$J^2=[J_1(\xi)-J_0(\xi)]^2 \tag{9}$$

with $\xi = K^2/(4+2K^2)$, L_{0k} being the length of the optical klystron, r the electronic density, F_f the filling factor representing the transverse overlap between the optical and electron pulses. The gain is increased for lower beam energies, high beam quality (low emittance), and long interaction region (long insertion device). Nevertheless, working at low energy on a storage ring dramatically reduces the Touschek lifetime, whereas several hours of lasing are required for an FEL source for users (of the order of 10 h in the Super-ACO case).

The gain varies with Nd, the interference order of the dispersive section, obtained by a simple change in the dispersive section gap, as illustrated in Fig. 14(a).

The gain also evolves with the current I [see Fig. 14(b)], and particularly changes below 20–30 mA. This results from the electronic density p variation with current, proportional to I/σ_1: above the threshold of anomalous bunch lengthening, the enhancement of σ_1 and I compensate; below, σ_1 increase due to potential well distortion being low; the gain evolution is mainly dominated by the increase of current. It can be approximated by

$$g=\begin{cases} g_{\text{off}} I/I_0 & \text{for } I<I_0 \ , \\ g_{\text{off}} & \text{for } I>I_0 \ , \end{cases} \tag{10}$$

with $g_{\text{off}}=2\%$ and $I_0=16$ mA. For $I>70$ mA, the gain relationship, based on a Gaussian distribution for the bunch distribution, is really approximative.

2. *Laser evolution and saturation*

The position of the laser micropulse or even of the stored spontaneous emission compared to the longitudinal distribution determines the gain for a given pass. Of course, the maximum gain occurs for the laser micropulse centered in the bunch distribution for a perfectly Gaussian beam, the slippage being neglectible. Nevertheless, it has been clearly observed that the bunch distribution can be asymmetrical, deviating from a Gaussian distribution. In addition, the perfect tuning condition (1 Hz over 100 MHz) is very difficult to keep for long, so the laser tuning condition can easily be modified after several passes. Such a situation can be modeled with the pass-to-pass longitudinal evolution [15]:

$$y_{n+1}(\tau)=R^2 y_n(\tau-\varepsilon)[1+g(\tau)]+i_s \ , \tag{11}$$

$y_n(\tau)$ being the longitudinal profile of the laser pulse, τ the longitudinal coordinate inside the micropulse (the origin being taken at the synchronous electron), R^2 the mirror reflectivity, ε the detuning with respect to the electron bunch, and i_s the spontaneous emission. The total laser dimensionless intensity I_1 is then given by

$$I_1(t)=\int_{-\infty}^{+\infty} y(t,\tau)d\tau \ . \tag{12}$$

The evolution of the energy spread is given by

$$\frac{dS}{dt}=2(I-\Sigma)/t_s \ ,$$

with $\Sigma=(\sigma\gamma/\gamma^2-\sigma\gamma/\gamma_{\text{off}}^2)/(\sigma\gamma/\gamma_{\text{eq}}^2-\sigma\gamma/\gamma_{\text{off}}^2)$, $\sigma\gamma/\gamma_{\text{eq}}$ standing for the energy spread without laser off and $\sigma\gamma/\gamma_{\text{eq}}$ with the laser at equilibrium. $\Sigma=I=1$ corresponds to the equilibrium condition. These equations represent the increase of laser intensity and the start of the generally admitted saturation process due to the energy redistribution in the bunch, called "bunch heating." The energy exchange between the positron bunches and the laser pulses modifies the energy distribution, and thus the longitudinal distribution of the positron bunch. With an ideal beam (without anomalous bunch lengthening), the laser interaction should "heat" the beam, enhance the energy spread, and consequently slightly enhance the bunch length [30].

In first approximation the longitudinal distribution profile of the electron bunch can be assumed to be Gaussian, so

$$g=g_0 \exp(-\tau^2/2\sigma_1^2) \tag{13}$$

the laser saturation results from the laser detuning process combined with the enhancement of the energy spread leading to the gain reduction according to

$$g_0=g_{\text{off}}(P/g_{\text{off}})^{\Sigma} \ , \tag{14}$$

g_{off} being the initial gain without laser and P the cavity losses ($P=1-R^2$). Here, in fact, a competition occurs between the phenomena responsible for the anomalous bunch lengthening and the laser heating, and the bunch length remains smaller than expected. No significant change was measured with the dissector.

The previous equations lead to the natural laser oscillating period,

$$T_r=2\pi(\tau_r\tau_s/2)^{1/2} \ . \tag{15}$$

According to the tuning condition and the relative values

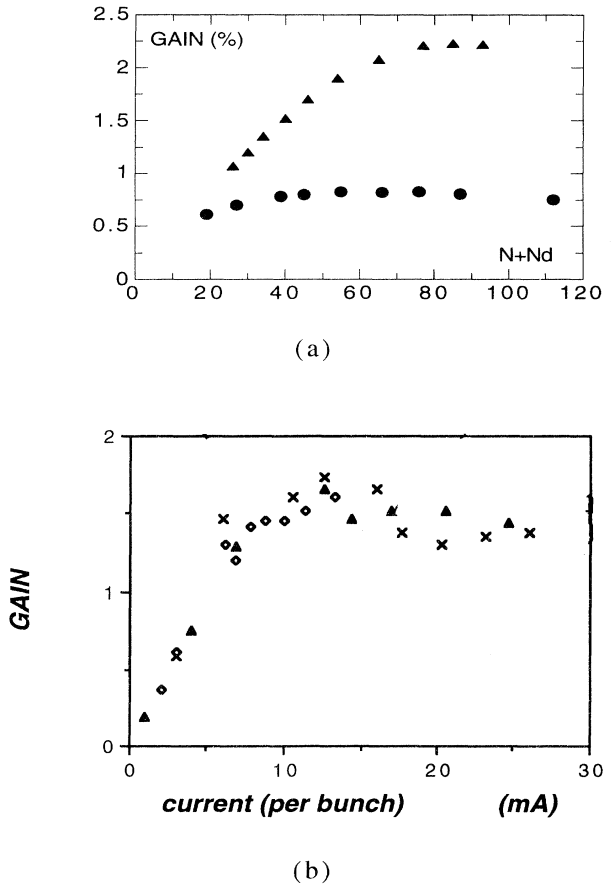

FIG. 14. FEL gain on Super-ACO: (a) vs the interference order of the dispersive section, experimental values at 600 MeV, 630 nm; (b) vs the bunch current, assuming a Gaussian shape.

of τ_r and τ_s, the response of the laser can be damped oscillator, leading to a cw regime (as in zones 1, 3, 5 for the Super-ACO FEL) or an oscillator of relaxation (as in zones 2 and 4).

In addition, according to (11), the saturation (corresponding to the gain evolution from its initial value to the losses level) can also result from the laser micropulse jittering [12] accumulated over passes, without great modification of the positron bunch distribution. Around the perfect tuning (corresponding to the maximum initial gain), the position of the Super-ACO FEL micropulse is changing rapidly for very small modification of the synchronization condition (as shown in the upper part of Fig. 1), so the gain partly decreases from the change of position of the micropulse compared to the bunch distribution, and from the enhancement of energy spread. Starting from a detuned condition, the initial gain is smaller and closer to the losses level, so the FEL micropulse is more maintained in its position and a very small increase of energy spread is sufficient to saturate. Such a phenomenon has only been observed on Super-ACO, because it is the only FEL being cw for a small detuning range around perfect synchronism, and the electron bunch distribution is rather wide. When the FEL is pulsed around perfect synchronism, it is much more difficult to dynamically follow the FEL micropulse position.

C. Laser micropulse narrowing

1. Laser micropulse width

The FEL gain is proportional to the electronic density, and the FEL builds for the maximum of gain at perfect synchronism, i.e., around the maximum of the longitudinal distribution of the positron bunch, or when the gain is equal to the losses when it is detuned (i.e., with a displacement of the center of the electronic distribution). The laser pulse, generated from the bunch longitudinal distribution, narrows it by a factor of 5–10, providing an improved source, compared to synchrotron radiation, for its temporal structure. When the laser is detuned, the FEL does not grow from the maximum electronic density, so more electrons are required to generate the laser, and the laser width is wider.

The streak camera measurements of the FEL distribution width (for various adjustments not too far from perfect synchronism) lead to an average value of the order of 25 ps rms, with extreme values of 8 and 44 ps. The histogram of the measurements is shown in Fig. 15.

This FEL micropulse width is smaller than the values obtained by other ways. The bigger width, measured with the dissector [15], i.e., 40 ps, results from the integration by the detector of the laser jitter (30 ps) deduced from the relationship

$$\sigma^2_{\text{diss}} = \sigma^2_{\text{streak}} + \Delta\tau^2_{\text{jitter}} .$$

Besides, the instrumental function of the time-resolved fluorescence performed on a biological sample [8] gave an rms value of 30 ps, after deconvolution with the estimated time-response of the electronics, for a FEL slightly detuned from perfect synchronism for stability requirements (without laser longitudinal feedback, see Sec. I and next section). As a consequence, there is a rather good agreement between the streak camera and the fluorescence experiments. The FEL micropulse width is then significantly narrower than the positron bunch from which it originates.

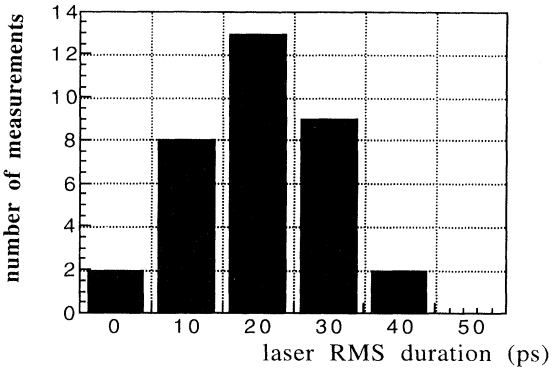

FIG. 15. Histogram of the laser micropulse measured with a streak camera.

Nevertheless, with a spectral width of the order of 0.4 Å [10,31], the FEL is not Fourier transformed, because the saturation process occurs too early, when the laser line has not reached its ultimate narrowing. Recent theoretical investigations show that the spectral and temporal narrowing of the FEL micropulse could continue towards the Fourier limit after the gain saturation, if the beam was stable enough during a sufficient time (ms to s) [10].

2. Behavior versus detuning and the dispersive section gap

As mentioned previously (see Sec. II), the position of the laser micropulse at perfect synchronism is very unstable; this jitter can detune the laser and modify its saturation. With more careful measurements of the FEL micropulse versus detuning [see Fig. 16(a)], it appears that the laser micropulse is minimum, of the order of 20 ps, for perfect synchronism in zone 3, and the width of its temporal distribution enhances smoothly with the desynchronization. The behavior is not completely symmetrical between zones 1 and 2 and zones 4 and 5, probably because of the asymmetry of the positron bunch distribution. The lengthening of the laser micropulse with the detuning results from a smaller electronic density, due to the nonperfect longitudinal overlap. Such a behavior has already been recorded with the dissector [see Fig. 16(b)] [17], but not so clearly, because of the convolution with the FEL jitter. From Fig. 16, the evolution versus detuning is similar for different gaps of the dispersive section, corresponding to various theoretical gains (actually, the experimental gain does not seem to

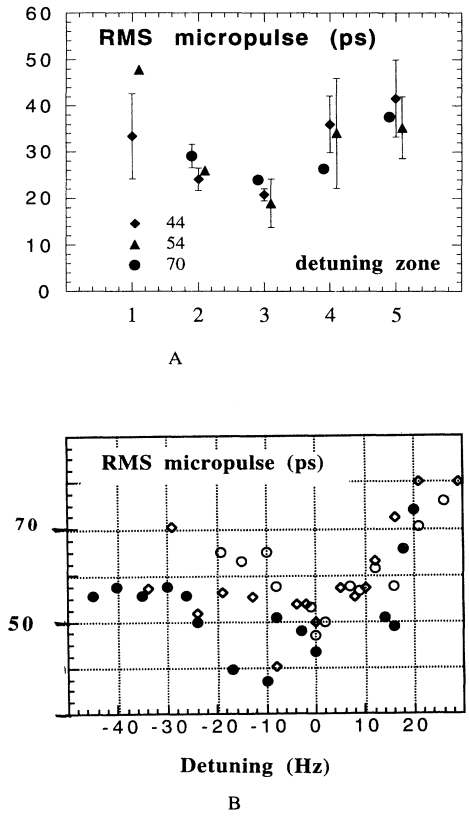

FIG. 16. rms FEL micropulse vs the detuning zone and the dispersive section gap. (a) Measurement performed with the streak camera. The errors bars correspond to the rms values of the measurements for each point. (b) Measurement performed with the dissector: full circles, gap of the dispersive section =43.5 mm and $N_d=79$; empty circles, gap SD=73 mm and $N_d=43$; lozenge, gap SD=75.4 mm and $N_d=41$.

depend on the dispersive section gap, except at threshold, as we could expect from theory).

3. *Laser micropulse evolution versus the stored current*

Figure 17 illustrates the laser micropulse for $I<20$ mA previously measured with the dissector. The laser micropulse width is reduced for a smaller current, which is probably related to a diminution of the width of the electronic density of the positron bunch. For laser threshold, the measurement gives 30–35 ps; that should, in reality, correspond to 15 ps, taking into account the widening due to the sampling of the dissector.

D. Effect of the FEL on the positron bunch of Super-ACO

1. *Longitudinal bunch distribution with the FEL*

The laser interaction leads to a small bunch "heating" of the positron bunch of Super-ACO. The bunch lengthening is smaller for a detuned FEL, where the saturation occurs more rapidly (see Fig. 18). The relative enhancement of the longitudinal bunch distribution width is smaller than the expected value considering the saturation by energy spread (70 ps), starting from an ideal distribution. Such a phenomenon has already been observed on the ACO FEL [32], with even a bunch shortening, resulting from a competition between the anomalous bunch lengthening and the laser heating. The measurements that were performed with the dissector gave more or less the same bunch length with and without laser. A complete theoretical model including all these phenomena is underway [33]. Greater bunch lengthenings were observed on VEPP3 and UVSOR.

2. *Effect on the synchrotron sidebands*

With high reflectivity mirrors, the laser has been established at rather high current (of the order of 120 mA) in the presence of strong and stable quadrupolar modes of oscillation. The laser destroys these quadrupolar modes and fluctuant hexapolar modes of synchrotron oscillations appear, so the laser heating competes with the phenomena responsible for coherent motion of a quadrupolar type. Maybe, according to the bunch lengthening due to the laser, the longer bunch is closer to a situation at higher current (where the hexapolar modes are present), but the synchrotron motion is nevertheless less coherent because of the redistribution of the electrons inside of the

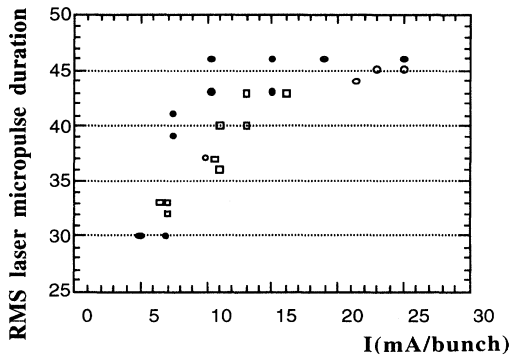

FIG. 17. Evolution of the laser micropulse width (in ps) vs the stored current (dissector measurement).

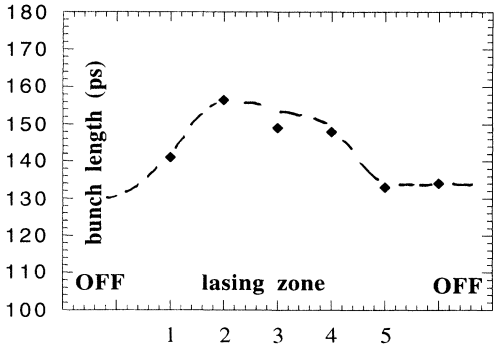

FIG. 18. Laser induced bunch lengthening measured with the streak camera.

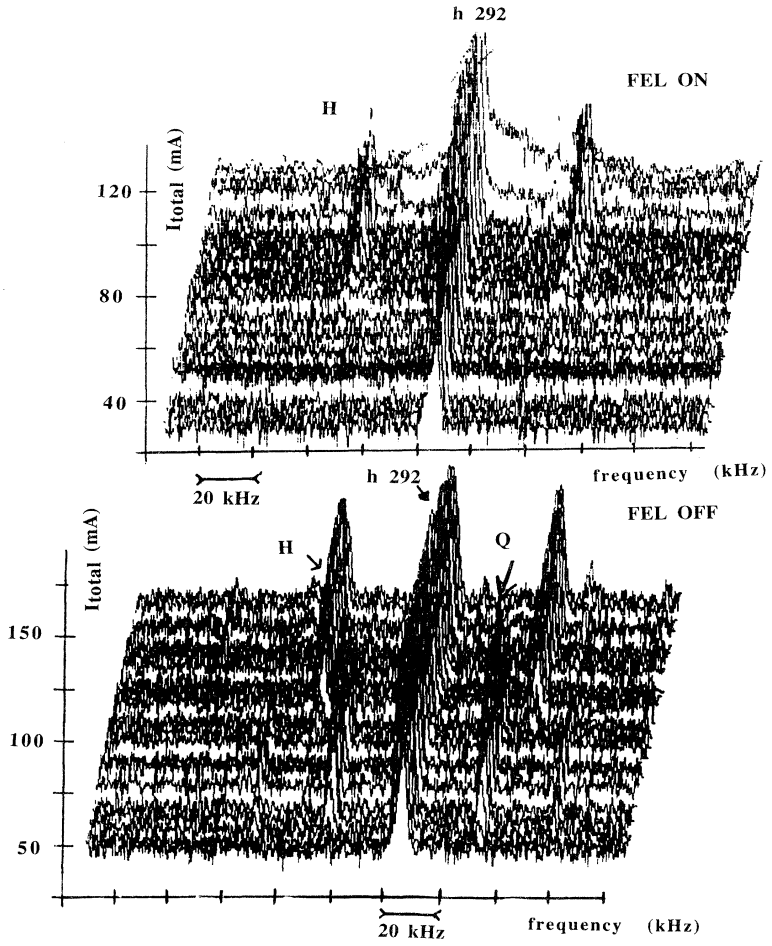

FIG. 19. Effect of the laser establishment on the synchrotron sidebands observed on the spectrum analyzer.

bunch due to the heating of the laser, so it could explain why fluctuant hexapolar lines appear. If the laser is stopped (mirror misalignment or desynchronization), the quadrupolar modes reappear (see Fig. 19). The laser induced bunch heating is in competition with the phenomena originating these quadrupolar modes. In addition, the laser establishment leads to a beam lifetime increase of the order of 1 h. A feedback system on the quadrupolar modes of synchrotron oscillations (based on a modulation of the rf voltage at the synchrotron frequency), under development, should allow the stabilization of the laser in the considered current range. The first preliminary tests showed no coherent motion on the beam with the laser when the quadrupolar modes were partially damped.

The FEL saturation on Super-ACO is in reality more complex than the presumed bunch lengthening from simple theories. Various effects, such as the coherent modes of synchrotron oscillations, beam excitation, relative values of the laser risetime, and synchrotron damping time in the ring can completely modify its dynamics. Consequently, its stability can also be affected by various sources of perturbation, as described in the next section.

V. THE SUPER-ACO FEL STABILITY

A. Under natural regime of operation

The Super-ACO FEL stability is first studied for natural lasing, mainly in zone 3, or slightly detuned in zones 1 and 5. The FEL stability is a very critical issue as far as using such a source is concerned. The analysis is restricted to temporal aspect, the spectral features being described elsewhere [31]. The laser jittering mentioned previously (cf. Sec. II), the possible modification of shape of the laser micropulse observed with the streak camera, and intensity fluctuations are detailed here.

1. Laser micropulse jitter

The micropulse jittering (FEL micropulse jittering around its reference position, corresponding to the center of mass of the positron bunch longitudinal distribution) previously observed with the dissector [17,19] was also measured with the streak camera. In Fig. 5, for example, the laser micropulses are not regularly spaced in time, although identical delays were applied to the synchroniza-

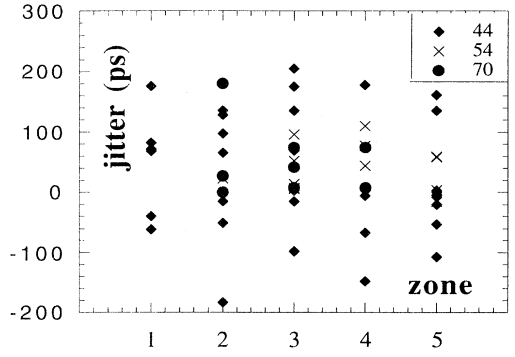

FIG. 20. Laser micropulse jitter vs detuning and dispersive section gap (44, 54, and 70 mm), measured with the streak camera.

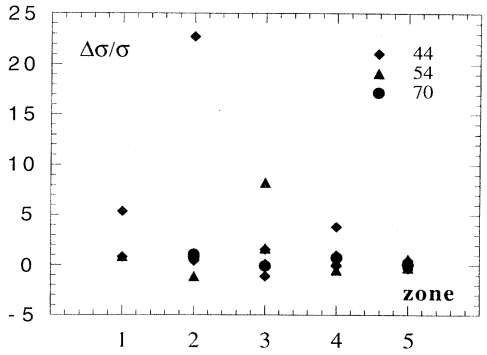

FIG. 21. Dissymmetry of the laser micropulse recorded with the streak camera vs detuning and the dispersive section gap; it is deduced from the moment $M3$ of the distribution.

tion of the streak camera. The jitter is maximum around perfect synchronism (see Fig. 1). It is partially responsible for the Super-ACO FEL saturation [15]. The stability of the synchronization of the streak camera has been properly checked with synchrotron radiation with two stable bunches stored in Super-ACO. In Fig. 20, the micropulse jitter decreases when the laser is detuned, and when the gain is smaller. It can reach as much as 200 ps, especially in zone 3 (see Fig. 1), where the position of the micropulse is significantly changing compared to a detuned laser, so the laser is much more sensitive to a perturbation and can jitter much more.

This jitter occurs at rather high frequency, as observed with the dissector (up to 1–10 kHz). Rapid changes could not really be attributed to mechanical distortion or dilatation, but more probably, to modifications of the longitudinal bunch distribution, or to sudden excitation or perturbation on the beam. This jitter is a real prejudice for time-resolved experiments using the FEL. To damp it, a longitudinal feedback system specifically designed has been developed [34], (see Sec. V B 1).

2. *Laser micropulse shape modification*

A single laser micropulse from the Super-ACO FEL, observed with the streak camera, does not always exhibit a Gaussian shape, as shown in Fig. 5: several single laser micropulses, artificially delayed by 500 ps, show different shapes, with quite a strong deviation from the Gaussian one. A change in shape and intensity is observed but the RMS value remains more or less identical. Such a phenomenon cannot be observed with the dissector, because of the averaging over many pulses. The structure in the micropulse could reveal the presence of several micropulses inside the same micropulse, as has been observed systematically on the UVSOR FEL [4]. In that case, the evolution of the macrotemporal structure has only three zones (with a pulsed laser for perfect synchronism) and the electron bunch is significantly shorter, resulting in a slightly different dynamics.

However, the observation of non-Gaussian laser micropulses does not occur systematically. The laser micropulse asymmetry deduced from the third moment of the distribution is illustrated in Fig. 21, for various conditions of laser operation. The dissymmetry is reduced for a detuned laser or for the laser operating at threshold (dispersive section at a gap of 70 mm). When the gain over losses is small, the laser saturates, whereas the pulse narrowing is still very small, but there is no possibility for various pulses to develop simultaneously because of the insufficient gain. When the gain is higher, several laser micropulses could probably develop together, and the laser dynamics is then very sensitive to perturbations. As the FEL micropulse is generally Gaussian, the structures probably do not result from an intrinsic feature of the super-ACO FEL dynamics. It might be due to some energy fluctuations, or changes in the longitudinal bunch distribution of the Super-ACO beam, especially with the structures observed on records of synchrotron radiation.

A real theoretical interpretation of these structures is, in fact, very complex, because it requires the complete study of the FEL dynamics, and in particular, the response of the system to various perturbations, such as modification of the current in the magnetic elements of the ring, of the rf cavity parameters (voltage, frequency change, etc.), of the cavity length. In addition, modeling a storage ring FEL is more complex than for a LINAC type FEL, because of the constant action of the FEL on the beam, and of the beam on the FEL. Preliminary results on correlation experiments to investigate the coupled spectral and temporal behavior seem to show that the laser features are very sensitive to the beam rapid changes, such as in energy or in the transverse motion.

3. *Laser micropulse intensity fluctuation*

Related to modifications of shape are observed intensity fluctuations on the laser micropulse. Figures 22(a)–22(c) give the intensity stability of the delayed pulses recorded on the same films, for various conditions of detuning. As previously observed with the dissector, it appears that the cw detuned laser is more stable in inten-

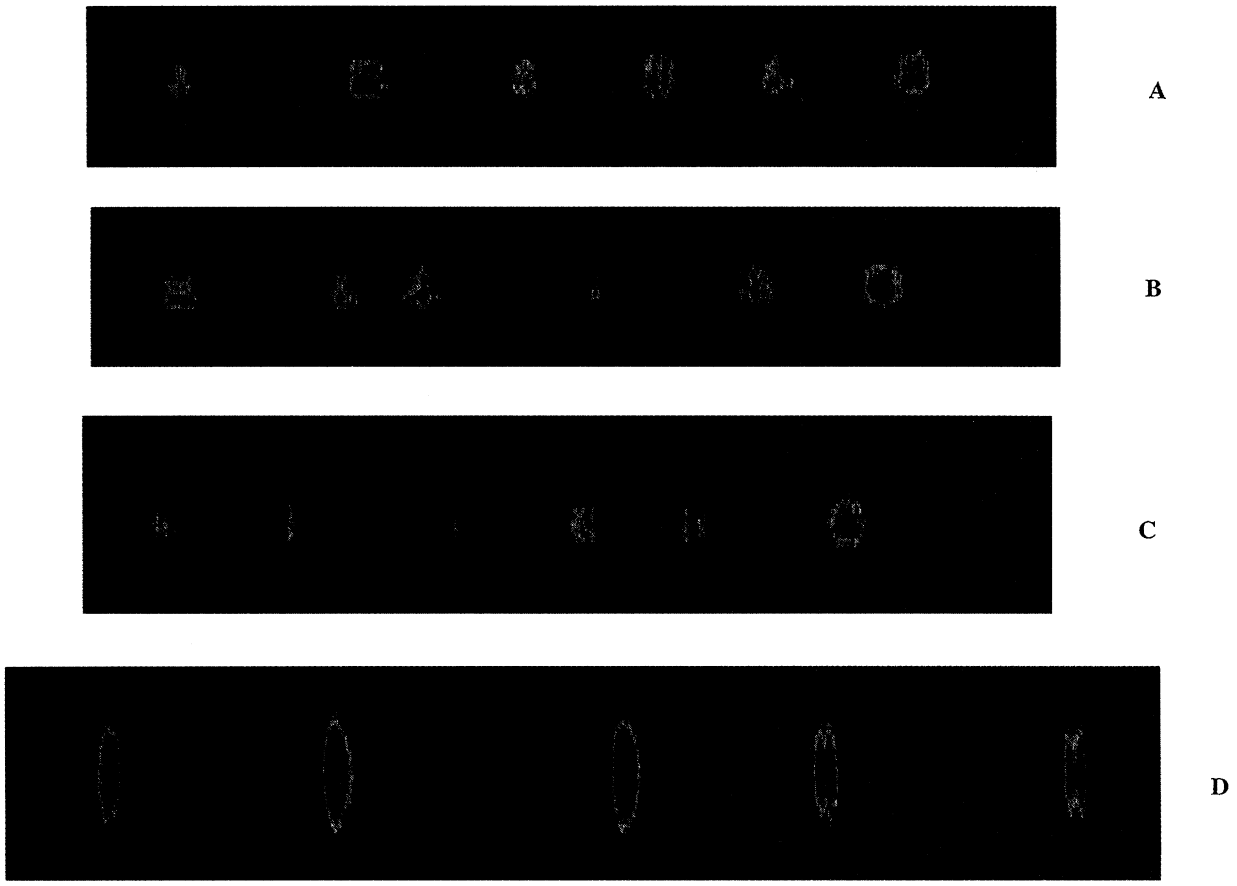

FIG. 22. Laser intensity contour vs detuning: (A) perfect tuning, (B) detuning of −3 Hz, (C) detuning of +9 Hz, (D) laser contour in the Q-switched mode.

sity and position.

The operation of the laser at high current (between 120 and 70 mA, with coherent synchrotron oscillations) leads to a general pulsed structure, generally on the line harmonics, for the whole detuning range [see Fig. 23(a)]. Exceptionally, a fine adjustment of the cavity mirrors and of the synchronization can lead to a cw FEL [see Fig. 23(b)]. In the usual range of current (70–20 mA), the laser is cw in the regions 1, 3, 5. In addition, for some specific beam injections a line modulation appears on the macrotemporal structure [see Fig. 23(c)], and no solution has been found so far to get rid of it.

B. Forced regimes of operation of the FEL

Here the stability of the FEL under forced regimes of operation, such as in presence of a longitudinal feedback [34], or in the Q-switched regime, is analyzed. Both modify the synchronization condition between the FEL light stored in the optical cavity and the bunches circulating in the ring, by slightly changing the revolution frequency of the particles.

1. Stabilization with a longitudinal feedback system

A longitudinal feedback system detecting the temporal change (see Fig. 24) of the FEL micropulse, with the dissector sampling at 300 Hz and readjusting the synchronization condition with the rf frequency, allowed the laser micropulse jitter, intensity fluctuations, and spectral drifts to be stabilized [34]. The sampling frequency of the dissector was recently upgraded from 50 Hz to 1 kHz in order to compensate rapid changes in synchronization. For a dissector operating at 300 Hz, the temporal jitter of the laser micropulse can be reduced to 10–50 ps, the spectral drift to less than the resolution of a scanning Fabry-Pérot (0.01 Å), and the intensity fluctuation down to 1% [see Fig. 23(e)]. The feedback can allow the laser to work without any readjustment during more than 3 h, as illustrated in Fig. 25 (stabilization over more than 3 h without any readjustment) with the applied voltage to the rf driver. One also observes from this figure the presence of sudden transient changes inducing a very rapid modification in the synchronization. Nevertheless, such results are achieved for a rather original stable beam, and

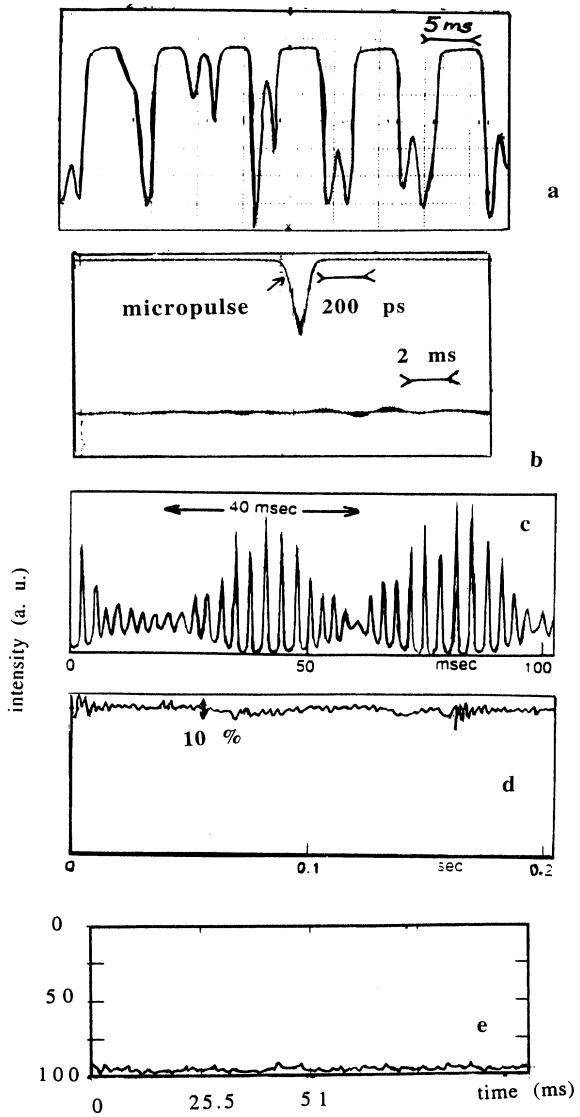

FIG. 23. Macrotemporal structure of the laser (a) at high current, pulsed structure, strongly synchronized on line, (b) cw regime, occurring for very specific conditions of detuning and mirror adjustment (88 mA), (c) case of double modulation derived from line (25 and 350 Hz), (d) natural lasing without feedback, (e) with the feedback system ($I < 70$ mA).

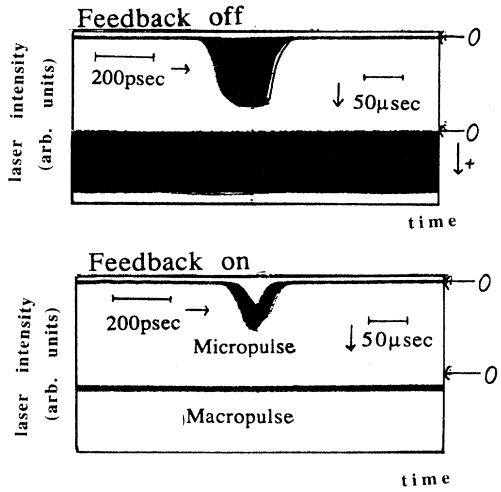

FIG. 24. Effect of the longitudinal feedback on the laser intensity and micropulse jitter.

it happens that, for some experiments, it is very difficult to stabilize the FEL, and the feedback is less efficient. The perturbations might be related to transverse instabilities on the laser, as one could suspect from the rapid modification of the laser transverse modes under such regimes. This point will be investigated further in the future. In addition, the feedback can only be established only below 70 mA, because of the presence of the quadrupolar modes of synchrotron oscillation above this threshold. The stabilization of these modes of synchrotron oscillation is really required in order to insure a reliable laser stability. However, the longitudinal feedback allows a better laser source to be provided, which can now be employed for use at perfect synchronism.

It could be mentioned that such a feedback can be really efficient at perfect synchronism in the case of a cw natural lasing for such tuning conditions. If the laser is pulsed in the central region, as on UVSOR [4], a feedback should be developed in the cw detuned region. Otherwise, one can Q-switch the laser at perfect tuning, but it introduces an additional macrotemporal structure, leading to different FEL features.

2. *Operation in the Q-switched mode*

The laser stability is generally improved in the Q-switched mode. An advantage can be taken from the natural oscillating laser frequency for operating the FEL in the Q-switched mode: the gain is artificially suppressed during 10–50 ms [31] by changing the revolution frequency in the ring by few hundreds of Hz, thus modifying the longitudinal overlap between the electron bunches and the optical pulses stored in the optical cavity, and suddenly reestablished. Thus, the laser starts from a nonperturbated situation, with a rise time of the order of 50 ms and presents a forced macrotemporal structure, a peak power enhanced by the order of 30, compared to the

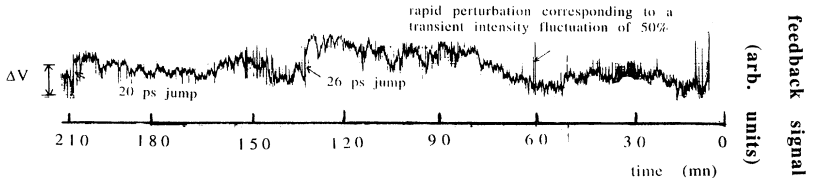

FIG. 25. Feedback signal vs time.

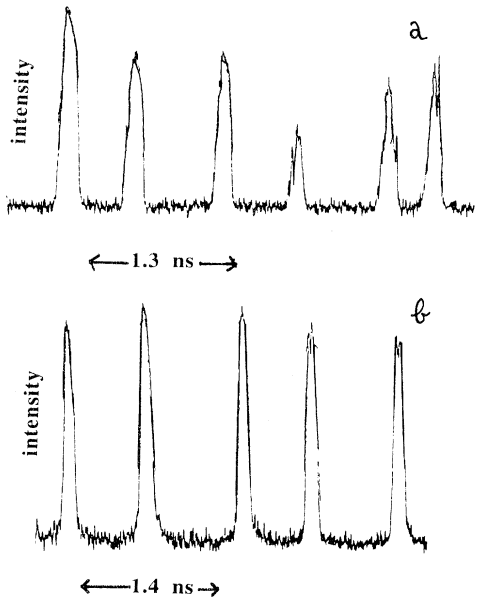

FIG. 26. Comparison between the laser in its natural mode of operation (a) and in the Q-switched mode (b).

natural mode, and the pulse to pulse intensity is more stable.

The measurement of the FEL in the Q-switched mode with the streak camera has been possible with the double synchronization between the laser micropulses and macropulses. This measurement is more difficult and less precise with the dissector, because the ramp and the gain modulations should be synchronized and the micropulse has to be deconvoluted from the laser macropulse.

The results obtained with the streak camera, which are illustrated in Fig. 26 and in the contour plot of Fig. 22, confirm the enhancement of peak power, show a more stable intensity, a shape closer to a Gaussian shape than in the natural regime. A detuning leads to an enhancement of the laser micropulse width, analogous to the behavior in the natural operation.

VI. CONCLUSION

It appears that the temporal dynamics of storage ring free electron laser sources is very complicated, sometimes involving the presence of several laser pulses inside the same micropulse and strongly related to the behavior of the positron bunch from which it is generated. A careful analysis requires the use of sophisticated detectors, such as dissectors and streak cameras. Nevertheless, the laser stability, which is very sensitive to any perturbation, can significantly be improved with the help of feedback systems, providing thus a tunable source of a high stability for various applications.

ACKNOWLEDGMENTS

The authors would like to especially thank D. Schirman (CEA-Limeil) for letting us have the opportunity to install for a few months the streak camera on the FEL sight. P. Silvin (CEA-Limeil) helped us with treating the films at the microdensitometer, and P. Herbert (CEA-Limeil) helped us with the software modification concerning the moments methods. The authors are also indebted to E. Zinin (Budker Inst. Novosibirsk), who installed the dissector on the Super-ACO experiment. Finally, R. Bakker participated in some figure elaboration and final dissector measurements.

[1] D. A. G. Deacon, L. R. Elias, J. M. J. Madey, G. L. Ramian, H. A. Schwettman, and T. I. Smith, Phys. Rev. Lett. **38**, 892 (1977).

[2] M. E. Couprie, M. Billardon, M. Velghe, C. Bazin, J. M. Ortega, R. Prazeres, and Y. Petroff, Nucl. Instrum. Methods A **296**, 13 (1990); M. E. Couprie, M. Velghe, R. Prazeres, D. Jaroszynski, and M. Billardon, Phys. Rev. A **44**, 1301 (1991); M. E. Couprie, M. Billardon, M. Velghe, and R. Prazeres, Nucl. Instrum. Methods A **304**, 53 (1991); M. E. Couprie, D. Garzella, A. Delboulbé, M. Velghe, and M. Billardon, Europhys. Lett. **21**(9), 909 (1993); M. E. Couprie, Ph.D., University of Paris–Sud, 1989 (unpublished).

[3] G. N. Kulipanov, I. V. Pinaev, V. M. Popik, A. N. Skrinsky, A. S. Sokolov, and N. A. Vinokurov, Nucl. Instrum. Methods A **296**, 1 (1990); M. E. Couprie, N. G. Gavrilov, G. N. Kulipanov, V. N. Litvinienko, I. V. Pinaev, V. M. Popik, A. N. Skrinsky, and N. A. Vinokurov, *ibid.* **304**, 47 (1991).

[4] S. Takano, H. Hama, and G. Isoyama, UVSOR Activity Report 1992 (unpublished); H. Hama, J. Yamazaki, and G. Isoyama, Nucl. Instrum. Methods A **341**, 12 (1994); H. Hama, J. Yamazaki, T. Kinoshita, K. Kimura, and G. Isoyama, *ibid.* **358**, 365 (1995).

[5] T. Yamazaki, K. Yamada, S. Sugiyama, H. Ohgaki, N. Sei, T. Mikado, T. Noguchi, M. Chiwaki, R. Suzuki, M. Kawai, M. Yokoyama, K. Owaki, S. Hamada, K. Aizawa, Y. Oku, A. Iwata, and M. Yoshiwa, Nucl. Instrum. Methods A **331**, 27 (1993).

[6] P. G. O'Shea, S. C. Bender, D. A. Byrd, J. W. Early, D. W. Feldman, C. M. Fortgang, J. C. Goldstein, B. E. Newnam, R. L. Sheffield, R. W. Warren, and T. J. Zaugg, Nucl. Instrum. Methods A **341**, 7 (1994).

[7] M. E. Couprie and N. Billardon, J. Phys. (France) IV, C9-327 (1994).

[8] M. E. Couprie, P. Tauc, F. Merola, A. Delboulbé, D. Garzella, T. Hara, and M. Billardon, Rev. Sci. Instrum. **65**(5), 1485 (1994).

[9] M. E. Couprie, *Applications of Free Electron Lasers in the UV,* Proceedings of the Symposium on Ion and Laser Processing for Advanced Materials, Oct. 1994, Keihanna, Japan, edited by T. Takagi and T. Tominasu (unpublished).

[10] Thèse T. Hara, Ph.D. dissertation, Université Paris–Sud, 1995.

[11] M. Marsi, R. Bakker, M. E. Couprie, A. Delboulbé, D. Garzella, T. Hara, G. Indlekofer, L. Nahon, A. Taleb-Ibrahami, and M. Billardon, *Time Dependence of the FEL-induced Surface Photovoltage on Semi-conductor Interfaces Measured with Synchrotron Radiation Photoemission Spectroscopy,* 2nd FEL User Workshop, New York, 1995 (unpublished).

[12] D. Gontier and P. Troussel, Commissariat à l'Energie Atomique, Report No. EPL/022/93, 1993 (unpublished); M. E. Couprie, D. Gontier, P. Troussel, T. Hara, A. Delboulbé, and M. Billardon, Commissariat à l'Energie Atomique, DSM/DRECAM/SPAM Report No. 93/377, 1993 (unpublished); T. Hara, M. E. Couprie, A. Delboulbé, P. Troussel, D. Gontier, and M. Billardon, Nucl. Instrum. Methods A **341**, 21 (1994).

[13] P. Elleaume, J. Phys. **45**, 997 (1984).

[14] M. Billardon, Phys. Rev. Lett. **65**, 713 (1990).

[15] M. Billardon, D. Garzella, and M. E. Couprie, Phys. Rev. Lett. **69**(16), 2368 (1992); M. E. Couprie, D. Garzella, A. Delboulbé, M. Velghe, and M. Billardon, Nucl. Instrum. Methods A **331**, 84 (1993); M. E. Couprie, D. Garzella, A. Delboulbé, M. Velghe, and M. Billardon, *ibid.* **331**, 37 (1993).

[16] E. I. Zinine, Nucl. Instrum. Methods A **208**, 439 (1983).

[17] M. E. Courpie, V. M. Popik, E. I. Zinine, A. Delboulbé, D. Garzella, M. Velghe, and M. Billardon, Nucl. Instrum. Methods A **318**, 59 (1992); D. Garzella, *Studio della dinamica del laser a elettroni liberi sull' anello di accumulazione Super-ACO,* Tesi di laurea dell' universita degli studi di Pisa, March 1993.

[18] P. Troussel, Etalonnage absolu du film type 2484; ADONIS, software developed in Limeil.

[19] N. A. Vinokurov and A. M. Skrinsky (unpublished).

[20] M. E. Couprie, C. Bazin, and M. Billardon, Nucl. Instrum. Methods A **278**, 788 (1989).

[21] M. Sands, Stanford Linear Accelerator Center, Report No. 121, 1970 (unpublished).

[22] A. Nadji, P. Brunelle, M. P. Level, M. Sommer, and H. Zyngier, *Quasi-Isochronous Optics for Super-ACO* EPAC 94 (World Scientific, Singapore, 1994), Vol. 1, pp. 128–132.

[23] J. L. Laclare, CERN Report No. 264-326, 1987 (unpublished).

[24] J. C. Besson, P. Certain, A. Daël, P. Juan, A. Labèque, M. P. Level, P. C. Marin, C. Monet-Descombey, P. Nghiem, M. Sommer, R. Souchet, and H. Zyngier, Anneaux Report No. RT/88-01, 1988 (unpublished).

[25] A. Hofman, CERN Accelerator School Report, 1977 (unpublished); B. Zotter and F. Sacherer, CERN Accelerator School Report, 1977 (unpublished); F. Sacherer, IEEE Trans. Nucl. Sci. **NS-20**, 825 (1973); **NS-24**, 1393 (1977).

[26] F. Pedersen and F. Sacherer, IEEE Trans. Nucl. Sci. **NS-24**, 1396 (1977); B. Kriegbaum and F. Pedersen, IEEE Trans. Nucl. Sci. **NS-24**, 1695 (1977).

[27] M. E. Couprie and M. Billardon, IEEE J. Quantum Electron. **30**, 781 (1994).

[28] A. Anders, *Bunch Length Measurements at the BESSY Storage Ring,* Proceedings of European Particle Accelerator Conference 92, (Editions Frontières, Berlin, 1992), Vol. 1, pp. 798–800.

[29] M. E. Couprie, M. Velghe, D. Jaroszynski, and M. Billardon, Nucl. Instrum. Methods A **304**, 58 (1991).

[30] A. Renieri, Nuovo Cimento B **59**, 160 (1979).

[31] T. Hara, M. E. Couprie, A. Delboulbé, D. Garzella, L. Nahon, and M. Billardon, Nucl. Instrum. Methods A **358**, 341 (1995).

[32] M. E. Couprie and P. Elleaume, Nucl. Inst. Methods Phys. Res. A **259**, 77 (1987).

[33] G. Dattoli, L. Giannessi, and A. Renieri, Nucl. Instrum. Methods A **358**, 338 (1995).

[34] M. E. Couprie, D. Garzella, T. Hara, J. H. Codarbox, and M. Billardon, Nucl. Instrum. Methods A **358**, 374 (1995).

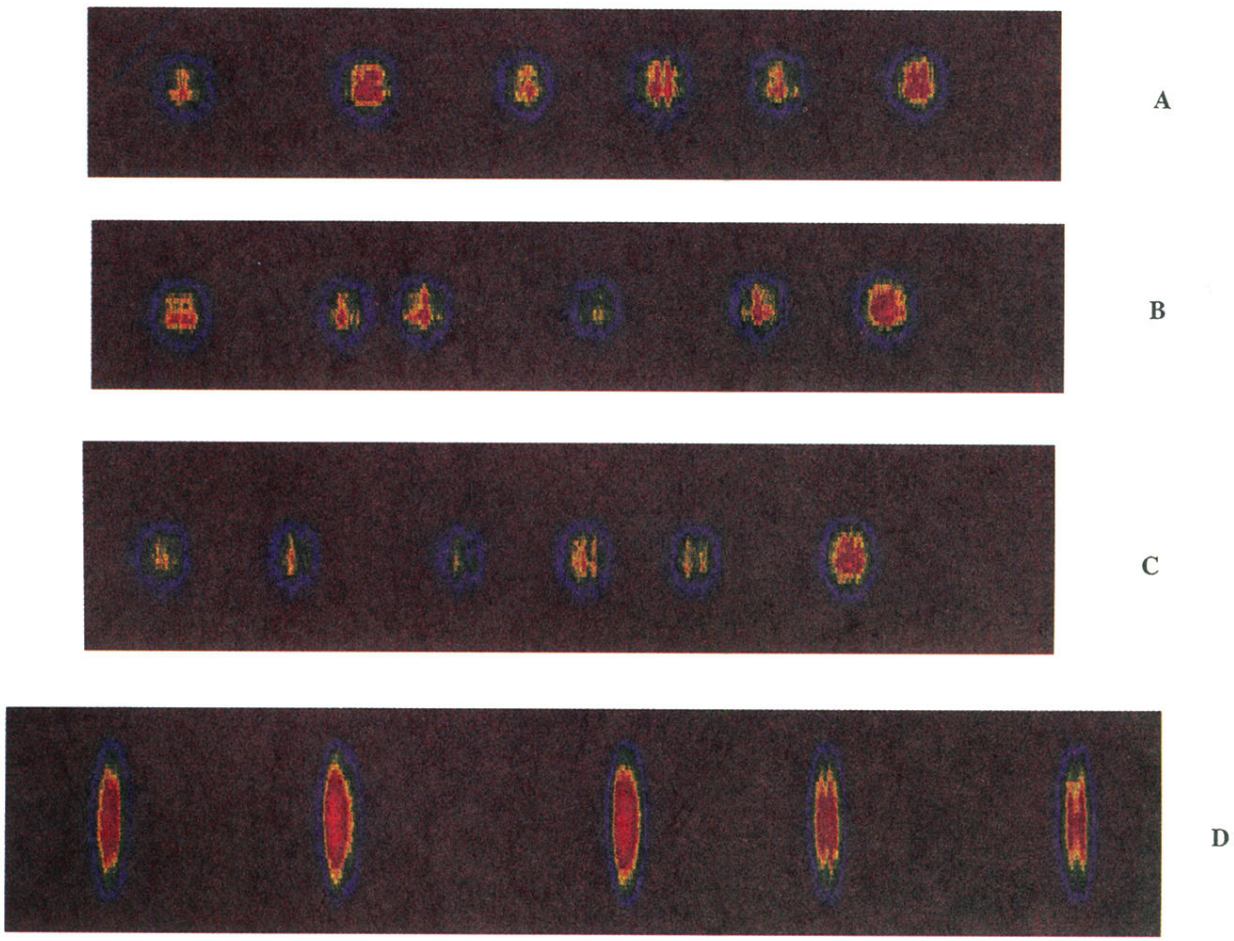

FIG. 22. Laser intensity contour vs detuning: (A) perfect tuning, (B) detuning of -3 Hz, (C) detuning of $+9$ Hz, (D) laser contour in the Q-switched mode.

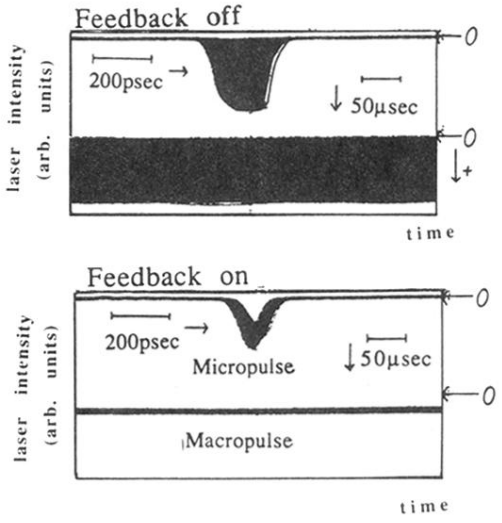

FIG. 24. Effect of the longitudinal feedback on the laser intensity and micropulse jitter.

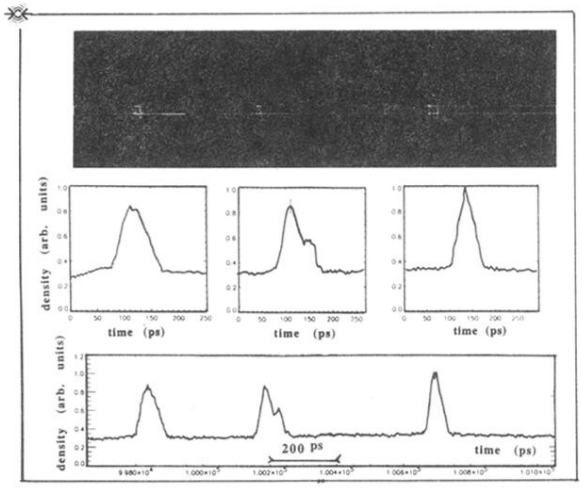

FIG. 5. Example of density profile and intensity laser distribution, this latter analyzed by the moments method. Several FEL micropulses are viewed, which were registered after applying an artificial delay.